

THE SPATIAL ENERGY SPECTRUM OF MAGNETIC FIELDS IN OUR GALAXY

J. L. HAN¹, K. FERRIERE², AND R. N. MANCHESTER³
 July 11, 2018

ABSTRACT

Interstellar magnetic fields exist over a broad range of spatial scales, extending from the large Galactic scales (~ 10 kpc) down to the very small dissipative scales ($\ll 1$ pc). In this paper, we use a set of 490 pulsars distributed over roughly one third of the Galactic disk out to a radius $R \simeq 10$ kpc (assuming $R_\odot = 8.5$ kpc) and combine their observed rotation and dispersion measures with their estimated distances to derive the spatial energy spectrum of the Galactic interstellar magnetic field over the scale range $0.5 - 15$ kpc. We obtain a nearly flat spectrum, with a 1D power-law index $\alpha = -0.37 \pm 0.10$ for $E_B(k) = Ck^\alpha$ and an rms field strength of approximately $6 \mu\text{G}$ over the relevant scales. Our study complements the derivation of the magnetic energy spectrum over the scale range $0.03 - 100$ pc by Minter & Spangler (1996), showing that the magnetic spectrum becomes flatter at larger scales. This observational result is discussed in the framework of current theoretical and numerical models.

Subject headings: ISM: magnetic fields — pulsars: general — turbulence

1. INTRODUCTION

On the whole, the physical properties of the interstellar gas are better established and understood than those of the interstellar magnetic field. The spatial power spectrum of interstellar HI has been measured using observations of the 21-cm line in several small areas across the sky. Emission measurements suggest a smooth power-law behavior with a 3D spectral index $\simeq -3$ for spatial scales $\gtrsim 5$ pc (e.g., Crovisier & Dickey 1983; Green 1993; Dickey et al. 2001), while 21-cm absorption measurements yield a 3D spectral index $\simeq -2.75$ in the scale range $0.01 - 3$ pc (Deshpande et al. 2000).

The spatial structure of interstellar free electrons has been probed using observations of Galactic pulsars and extragalactic compact sources. Relying on interstellar scintillation data, Armstrong et al. (1995) showed that the spatial power spectrum of the interstellar free-electron density in the nearby interstellar medium (ISM) could be approximated by a single power law with a 3D spectral index $\simeq -3.7$ (very close to the Kolmogorov value of $-11/3$) for scales ranging from $\sim 10^{10}$ cm to $\sim 10^{15}$ cm. By combining their scintillation data with rotation measure (RM) fluctuation measurements and with gradients in the average electron density, they were able to extend the range of their observed nearly-Kolmogorov spectrum up to a scale $\sim 10^{20}$ cm (~ 30 pc).

Studies of pulsar and extragalactic radio-source RMs have yielded a wealth of observational information on the spatial structure of the Galactic interstellar magnetic field. However, most studies to date have focused on the large-scale field structure (Simard-Normandin & Kronberg 1980; Han & Qiao 1994; Rand & Lyne 1994; Indrani & Deshpande 1998; Han et al. 2002) and only a few have provided estimates for the rms amplitude and the characteristic scale length of the turbulent magnetic field. For instance, by adopting a single-cell-size model for the turbulent field and analyzing the residuals with respect to their best-fit model for the large-scale field, Rand & Kulkarni (1989) obtained a turbulent field strength of $\simeq 5 \mu\text{G}$ and a cell size of $\simeq 55$ pc. Ohno & Shibata (1993), who did not resort to

large-scale field models, organized their pulsar data by pairs of pulsars seen in nearly the same direction and interpreted them in the framework of a single-cell-size model for the random field. With an assumed cell size in the range $10 - 100$ pc, they obtained a random field of amplitude $4 - 6 \mu\text{G}$.

As Rand & Kulkarni (1989) themselves acknowledged, the turbulent magnetic field cannot be satisfactorily described by a single scale length. Simonetti et al. (1984) and Simonetti & Cordes (1986) were the first authors to look into the question of how the turbulent magnetic energy in the ISM is actually distributed in the scale range $\sim 0.01 - 100$ pc. They used the structure function of RMs of extragalactic sources to investigate variations in the composite quantity $n_e \mathbf{B}$, where n_e is the free-electron density and \mathbf{B} is the magnetic field. Their study suggests that the 3D spatial power spectrum of fluctuations in $n_e \mathbf{B}$ at scales $\gtrsim 0.01$ pc can be described by a power law of index ~ -3.1 with an outer scale estimated at $\lesssim 90$ pc. Later, Minter & Spangler (1996) performed a combined analysis of the structure functions of RM and emission measure (EM) to separate the fluctuations in electron density and magnetic field in the scale range $\sim 0.03 - 100$ pc. They measured the RMs of 38 extragalactic sources located in a small area of the sky near Galactic coordinates $l = 144^\circ$, $b = 21^\circ$, where the EMs were deduced from measured $H\alpha$ intensities. For scale sizes up to ~ 4 pc, the structure functions of RM and EM were consistent with a 3D-turbulence model in which both electron density and magnetic field fluctuations have Kolmogorov spectra. Between ~ 4 pc and ~ 80 pc, the structure functions were consistent with 2D turbulence. Minter & Spangler (1996) also obtained an rms amplitude of $\sim 1 \mu\text{G}$ for the turbulent magnetic field on scales up to 4 pc.

It is clear that the magnetic energy spectrum does not abruptly stop at the estimated outer scale of the turbulence, ~ 80 pc. The spectral energy of the magnetic field will extend continuously up to the largest Galactic scales, as a result of an inverse cascade of magnetic helicity (e.g., Pouquet et al. 1976) and/or due to other physical processes involving compression and shearing at large scales (e.g., Parker 1971; Kulsrud 1986). Turbulent field and the more structured field at larger scales describe the present-day properties of the Galactic magnetic field and provide the necessary observational reference for theoretical models. Knowledge of the complete magnetic energy spectrum can offer a solid observational test for dynamo and other theories

¹ National Astronomical Observatories, Chinese Academy of Sciences, Jia 20 DaTun Road, Beijing 100012, China. Email: hjl@bao.ac.cn

² Observatoire Midi-Pyrénées, 31400 Toulouse, France. Email: ferriere@ast.obs-mip.fr

³ Australia Telescope National Facility, CSIRO, PO Box 76, Epping, NSW 1710, Australia. Email: Dick.Manchester@csiro.au

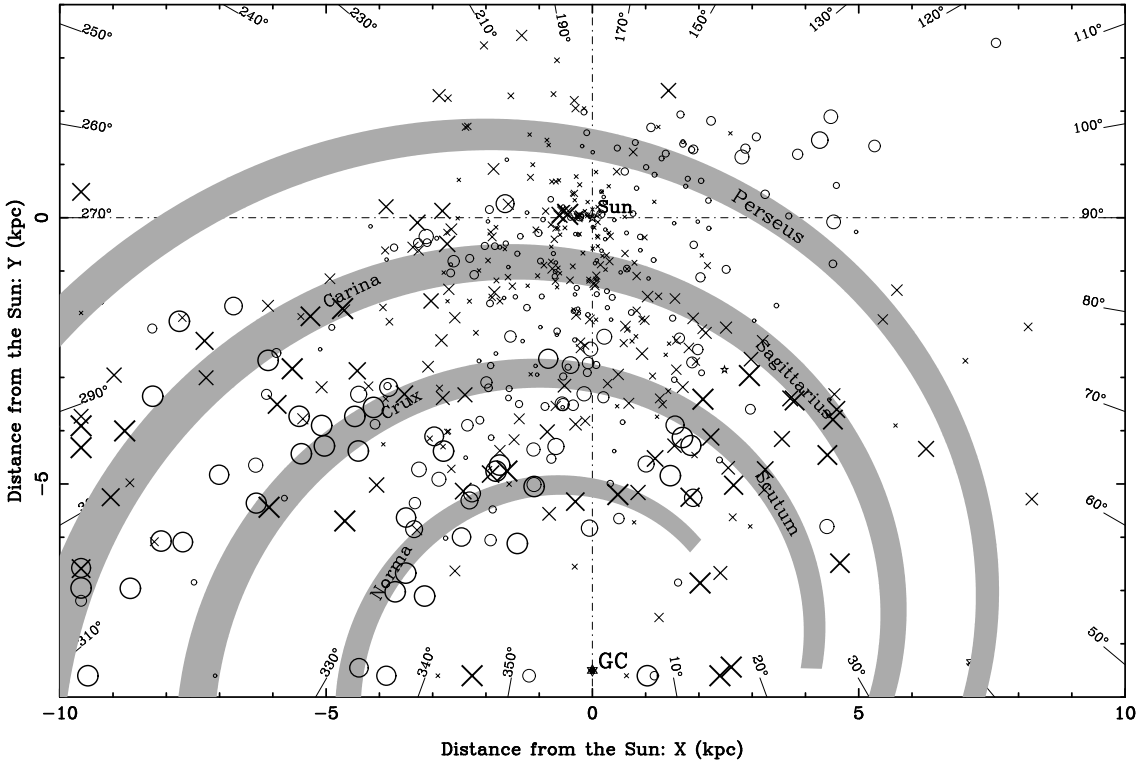


FIG. 1.— Distribution projected on the Galactic plane of the 490 pulsars with well-determined RMs viewed from the North Galactic pole. Pulsars with a positive RM are denoted with crosses, those with a negative RM are denoted with circles, and the symbol area is proportional to the RM. Superimposed onto the pulsar distribution is an approximate outline of the four known spiral arms.

for the origin of Galactic magnetic fields.

The purpose of the present paper is to determine the portion of the magnetic spectrum that lies above the strictly turbulent domain, thereby filling the observational gap between the large Galactic scales and the small turbulent scales. Pulsars are unique in providing a direct measure of the average line-of-sight component of the interstellar magnetic field, weighted by the local electron density, from the ratio of RM and dispersion measure (DM). Here we will analyse the available pulsar RM and DM data in combination with their estimated distances to deduce the interstellar magnetic energy spectrum E_B across the scale range 0.5 – 15 kpc. In § 2, we present our pulsar data and explain how they are used to construct the interstellar magnetic energy spectrum, in § 3, we review the assumptions underlying our derivation, and in § 4, we discuss the significance of our results and compare them with theoretical predictions.

2. THE MAGNETIC ENERGY SPECTRUM FROM PULSAR DATA

2.1. Derivation of $\langle E_{B_{\parallel}} \rangle(S)$

At the present time, we have 521 pulsars with measured RMs at our disposal: 330 of them are published measurements mostly from Hamilton & Lyne (1987); Rand & Lyne (1994); Qiao et al. (1995) and Han et al. (1999), while another 202 RMs come from unpublished observations with the Parkes telescope (see Han et al. 2002). We discard all pulsars with a RM uncertainty larger than 30 rad m⁻², leaving us with a set of 490 pulsars. The distances to the pulsars are determined from their DM using the NE2001 model for the Galactic electron density distribution (Cordes & Lazio 2003). The spatial distribution of our 490 pulsars is displayed in Figure 1, showing that they cover roughly one third of the thick ISM disk out to a Galactocentric

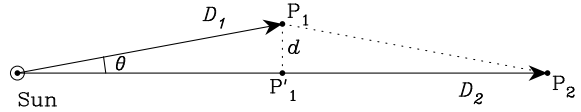


FIG. 2.— Geometry of paired pulsars P_1 and P_2 . \odot indicates the position of the Sun and P'_1 represents the projection of P_1 onto the line of sight to P_2 .

radius $R \sim 10$ kpc.

The average line-of-sight component of the interstellar magnetic field between a pulsar (P) and the Sun (\odot), weighted by the local free-electron density, is given by the ratio of the pulsar's RM to its DM:

$$\overline{B_{\parallel}}^P = \frac{\int_0^D n_e B_{\parallel} dl}{\int_0^D n_e dl} = (1.232 \mu\text{G}) \frac{RM}{DM}. \quad (1)$$

Here, n_e is the free-electron density (in cm⁻³), B_{\parallel} is the line-of-sight component of the magnetic field (in μG), dl is the length element along the line of sight to the pulsar (in pc), D is the distance to the pulsar (in pc), and DM and RM are expressed in pc cm⁻³ and in rad m⁻², respectively. Likewise, the electron-weighted average value of B_{\parallel} between two pulsars, P_1 and P_2 , located on the same line of sight is given by

$$\overline{B_{\parallel}}_{P_1}^{P_2} = (1.232 \mu\text{G}) \frac{RM_2 - RM_1}{DM_2 - DM_1}. \quad (2)$$

In order to extract as much information as possible on the spatial variations of the interstellar magnetic field, we are going to use both equation (1) applied to individual pulsars and equation (2) applied to pairs of pulsars lying in *almost* the same direction. Here, two pulsars P_1 and P_2 are considered to lie in almost the same direction if their angular separation, θ , satisfies

$$d|_{P_1}^{P_2} = D_1 \sin \theta < 0.1 \min(D_1, D_2 - D_1), \quad (3)$$

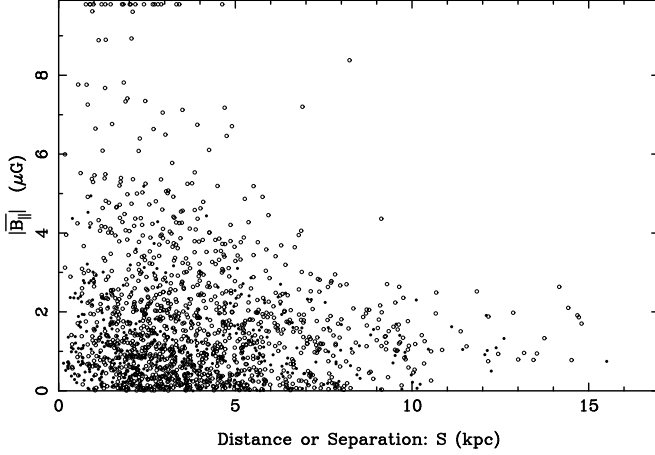


FIG. 3.— Measured values of $|\overline{B}_{\parallel}|$ as a function of S , where S is either the pulsar distance or the separation of pulsar pairs. The 490 filled circles correspond to measurements to individual pulsars while the 1200 open circles correspond to measurements between paired pulsars.

supposing that P_1 is the closer pulsar (see Figure 2). As we will see from equation (13) and Figure 5 below, $\overline{B}_{\parallel}|_{P_1}^{P_2}$ is only sensitive to magnetic fluctuation cells with sizes $\gtrsim 0.1S$ (where $S = D_1$ or $D_2 - D_1$). Equation (3) ensures that line segments $\odot P_1$ and $\odot P_1'$ pass through the same magnetic fluctuation cells with sizes $\gtrsim 0.1S$. The maximum angular separation between two paired pulsars is 5.7° . Note that our pair-selection approach is similar to that originally proposed by Ohno & Shibata (1993) for estimating the rms amplitude of the random field.

Altogether, we have 490 measurements of \overline{B}_{\parallel} to individual pulsars and 1200 measurements between paired pulsars. For the following, we denote by S the distance over which \overline{B}_{\parallel} is measured, i.e., $S = D$ for the first type of measurements and $S = D_2 - D_1$ for the second type. Measured values of $|\overline{B}_{\parallel}|$ are shown as a function of S in Figure 3. A few pulsar pairs had similar DMs but very different RMs, resulting in anomalously high values of \overline{B}_{\parallel} . In fact, the separation of these pulsars is almost certainly greater than indicated by the DMs, so these values were capped at $15 \mu\text{G}$. These and the few values between 10 and $15 \mu\text{G}$ are plotted at the top of the figure.

The magnetic energy associated with \overline{B}_{\parallel} for each pulsar or pulsar pair, $E_{\overline{B}_{\parallel}} \equiv \overline{B}_{\parallel}^2 / (8\pi)$, is plotted as a function of $k_S \equiv 1/S$ in Figure 4 on logarithmic scales. There is a wide scatter in the points, largely because, for any pulsar located at a given distance S and for any pair of pulsars separated by a given S , $|\overline{B}_{\parallel}|$ and $E_{\overline{B}_{\parallel}}$ can vary from zero to some maximum value depending on the angle between the line of sight and the direction of the local magnetic field as well as on the position of the pulsar or pulsar pair with respect to the maxima and minima of the magnetic fluctuations. Never-the-less, by averaging $E_{\overline{B}_{\parallel}}$ over successive intervals along the k_S -axis, we can obtain estimates for the mean value of the magnetic energy associated with \overline{B}_{\parallel} ,

$$\langle E_{\overline{B}_{\parallel}} \rangle = \left\langle \frac{\overline{B}_{\parallel}^2}{8\pi} \right\rangle, \quad (4)$$

as a function of k_S . It is important to realize that the above averaging procedure (denoted by angle brackets) implies averages over many different Galactic locations and many different lines of sight. Despite the wide scatter in $E_{\overline{B}_{\parallel}}$, the average values obtained for $\langle E_{\overline{B}_{\parallel}} \rangle$ (indicated with thick crosses in Figure 4) show

a clear trend with k_S , at least for $k_S \lesssim 2 \text{ kpc}^{-1}$. A least-squares fit of a power law to our estimated $\langle E_{\overline{B}_{\parallel}} \rangle$ gives

$$\langle E_{\overline{B}_{\parallel}} \rangle(S) = C_0 \left(\frac{k_S}{k_0} \right)^\beta, \quad (5)$$

with $\beta = 0.66 \pm 0.10$, $C_0 = (5.1 \pm 0.7) \times 10^{-13} \text{ erg cm}^{-3}$, $k_S = 1/S$, and the normalising factor $k_0 = 1 \text{ kpc}^{-1}$.

Individual pulsar distances are uncertain by $\sim 20\%$ or about 0.5 kpc at distances of a few kpc and there are only few pulsars within 0.5 kpc from the Sun. Therefore, our estimates for the parallel field strength and energy are unreliable at scales $\lesssim 0.5 \text{ kpc}$. In addition, there are only a few pulsars with distances greater than 15 kpc, so the range of validity of equation (5) is approximately $0.5 \text{ kpc} < S < 15 \text{ kpc}$.

2.2. Relationship between $\langle E_{\overline{B}_{\parallel}} \rangle(S)$ and $E_B(k)$

The next important step is to relate our measured $\langle E_{\overline{B}_{\parallel}} \rangle(S)$ to the magnetic-energy spectral density, $E_B(k)$. We proceed on the assumption (discussed in § 3) that the spatial fluctuations of the magnetic field, \mathbf{B} , are statistically homogeneous and isotropic. We start by writing $\mathbf{B}(\mathbf{r})$ in terms of its three-dimensional Fourier transform, $\tilde{\mathbf{B}}(\mathbf{k})$:

$$\mathbf{B}(\mathbf{r}) = \int \tilde{\mathbf{B}}(\mathbf{k}) e^{2\pi i \mathbf{k} \cdot \mathbf{r}} d\mathbf{k}, \quad (6)$$

where \mathbf{r} is the position vector and \mathbf{k} is the wave vector defined such that the relationship between wavenumber, k , and wavelength, λ , is $k = 1/\lambda$. The line-of-sight component of \mathbf{B} at a distance l can then be written as

$$B_{\parallel}(l) = \int \tilde{B}_{\parallel}(\mathbf{k}) e^{2\pi i k_{\parallel} l} d\mathbf{k}. \quad (7)$$

Its average value between two points located on the same line of sight at distances D_1 and D_2 , respectively, reads

$$\overline{B}_{\parallel} = \frac{1}{D_2 - D_1} \int_{D_1}^{D_2} B_{\parallel}(l) dl \quad (8)$$

or, after substitution of equation (7) and integration over l ,

$$\overline{B}_{\parallel} = \int \tilde{B}_{\parallel}(\mathbf{k}) \text{sinc}(\pi k_{\parallel} S) e^{2\pi i k_{\parallel} D_m} d\mathbf{k}, \quad (9)$$

with $S = D_2 - D_1$, $D_m = (D_1 + D_2)/2$, and $\text{sinc}(x) = (\sin x)/x$.

The expectation value of the magnetic energy associated with \overline{B}_{\parallel} may be defined as

$$\begin{aligned} \langle E_{\overline{B}_{\parallel}} \rangle(S) &= \frac{1}{8\pi} \langle \overline{B}_{\parallel} \overline{B}_{\parallel}^* \rangle \\ &= \frac{1}{8\pi} \int \int \langle \tilde{B}_{\parallel}(\mathbf{k}) \tilde{B}_{\parallel}^*(\mathbf{k}') \rangle \text{sinc}(\pi k_{\parallel} S) \text{sinc}(\pi k'_{\parallel} S) \\ &\quad e^{2\pi i (k_{\parallel} - k'_{\parallel}) D_m} d\mathbf{k} d\mathbf{k}'. \end{aligned} \quad (10)$$

In the last line of the above equation, the expectation value is applied to the factor $\tilde{B}_{\parallel}(\mathbf{k}) \tilde{B}_{\parallel}^*(\mathbf{k}')$, which is the only stochastic part of the expression. Now, for homogeneous and isotropic turbulence, we have

$$\begin{aligned} \frac{1}{8\pi} \langle \tilde{B}_{\parallel}(\mathbf{k}) \tilde{B}_{\parallel}^*(\mathbf{k}') \rangle &= \frac{1}{3} \left[\frac{1}{8\pi} \langle \tilde{\mathbf{B}}(\mathbf{k}) \cdot \tilde{\mathbf{B}}^*(\mathbf{k}') \rangle \right] \\ &= \frac{1}{3} \mathcal{E}_B(\mathbf{k}) \delta(\mathbf{k} - \mathbf{k}') \\ &= \frac{1}{3} \frac{E_B(k)}{4\pi k^2} \delta(\mathbf{k} - \mathbf{k}'), \end{aligned} \quad (11)$$

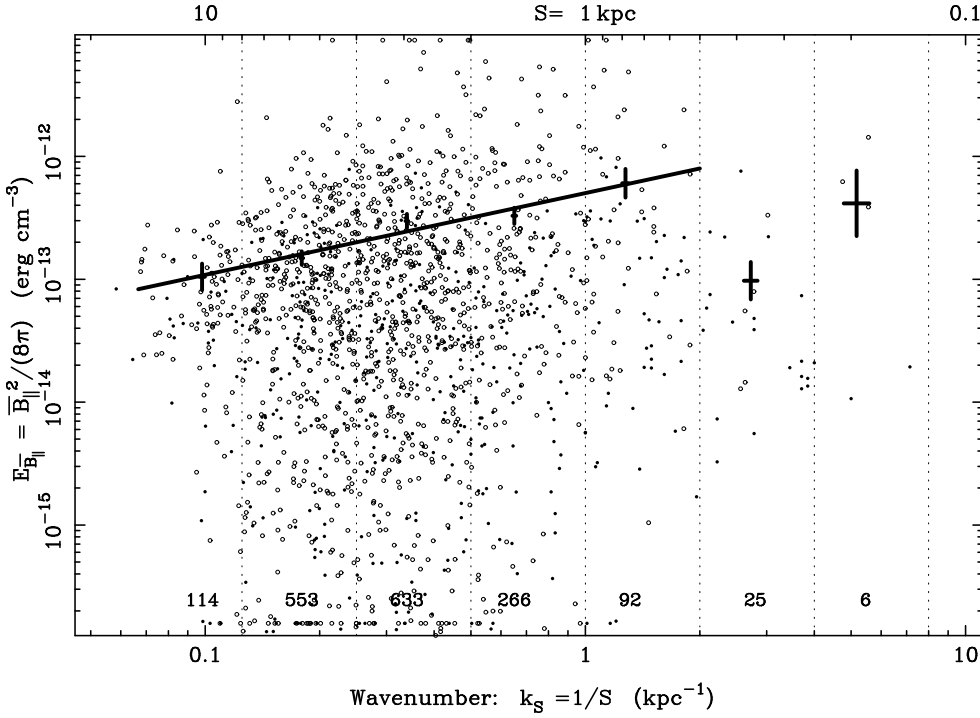


FIG. 4.— Measured values of the magnetic energy associated with $\overline{B_{\parallel}}$, $E_{\overline{B_{\parallel}}} = \overline{B_{\parallel}^2} / (8\pi)$, versus wavenumber, $k_S = 1/S$, where S is either the pulsar distance or the separation of pulsar pairs. The thick crosses give average values $\langle E_{\overline{B_{\parallel}}} \rangle$ and their uncertainties over the 7 successive intervals delimited by the vertical dotted lines and corresponding, from right to left, to $S(\text{kpc}) = [0.125, 0.25]$, $[0.25, 0.5]$, $[0.5, 1.0]$, $[1.0, 2.0]$, $[2.0, 4.0]$, $[4.0, 8.0]$, $[8.0, 16.0]$. The oblique thick line is a power-law fit to the $\langle E_{\overline{B_{\parallel}}} \rangle$ with $k_S < 2 \text{ kpc}^{-1}$ (see eq. [5]). The number of data points in each interval is indicated at the bottom.

where $\mathcal{E}_B(\mathbf{k})$ is the 3D magnetic-energy spectral density and $E_B(k)$ is its 1D counterpart. In view of equation (11), equation (10) reduces to

$$\langle E_{\overline{B_{\parallel}}} \rangle(S) = \frac{1}{3} \int \frac{E_B(k)}{4\pi k^2} \text{sinc}^2(\pi k_{\parallel} S) d\mathbf{k}. \quad (12)$$

The integration over the direction of \mathbf{k} is conveniently carried out in a cylindrical coordinate system with polar axis along the line of sight, such that $k_{\parallel} = k \cos \theta$ and $d\mathbf{k} = 2\pi k^2 dk d(\cos \theta)$. The final result can be cast in the form

$$\langle E_{\overline{B_{\parallel}}} \rangle(S) = \frac{1}{3} \int_0^{\infty} E_B(k) y(kS) dk, \quad (13)$$

with

$$y(kS) \equiv \frac{1}{\pi k S} \int_0^{\pi k S} \left(\frac{\sin x}{x} \right)^2 dx. \quad (14)$$

Clearly, the $1/3$ prefactor in equation (13) follows from our assumption of isotropy whereby one third of the magnetic energy goes into the line-of-sight component.

The shape of the weight function, $y(kS)$, is displayed for different values of the pulsar separation S in Figure 5. For any given S , magnetic fluctuations with $kS \ll 1$, i.e., with wavenumber $k \ll k_S$ or wavelength $\lambda \gg S$, give their full weight to $\langle E_{\overline{B_{\parallel}}} \rangle(S)$. Fluctuations with $k \sim k_S$ or $\lambda \sim S$ give approximately half their weight, and fluctuations with $k \gg k_S$ or $\lambda \ll S$ make a negligible contribution. Hence the main contribution to $\langle E_{\overline{B_{\parallel}}} \rangle(S)$ comes from fluctuations with wavenumber $k \lesssim k_S$. Physically, for long-wavelength fluctuations ($\lambda \gg S$), B_{\parallel} is nearly constant between both pulsars, so that its average value $\overline{B_{\parallel}}$ is approximately equal to its local value. For short-wavelength fluctuations ($\lambda \ll S$), B_{\parallel} reverses many times between both pulsars, so

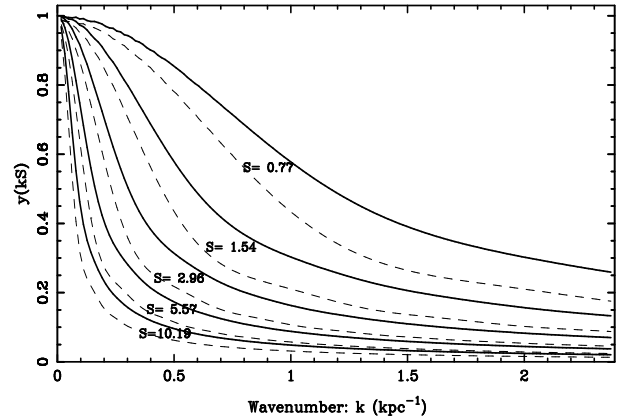


FIG. 5.— Weight function, $y(kS)$ (defined by eq. [14]), as a function of wavenumber, k , for 5 selected values of the pulsar separation, S (corresponding to the averaged S in the first 5 intervals of Figure 4), in the 3D case. The dashed lines show the weight function in the 2D case (eq. [16]).

that the contributions to $\overline{B_{\parallel}}$ from line segments with opposite sign of B_{\parallel} cancel each other out almost entirely. For fluctuations with $\lambda = S$, there is complete cancellation if \mathbf{k} is along the line of sight, and there is no cancellation if \mathbf{k} is perpendicular to the line of sight; an average over the direction of \mathbf{k} then leads to a net weight factor ~ 0.5 .

2.3. Determination of $E_B(k)$

In practice, we tried various analytical functions for $E_B(k)$. For each of them, we computed the corresponding function $\langle E_{\overline{B_{\parallel}}} \rangle(S)$ by integrating the right-hand side of equation (13) numerically and then compared the computed $\langle E_{\overline{B_{\parallel}}} \rangle$ to the mea-

sured $\langle E_{B_{\parallel}} \rangle$ displayed in Figure 4. The lower limit of integration as well as the step length of k were set to 0.02 kpc^{-1} . The upper limit of integration is mainly determined by the shape of the weight function, $y(kS)$, shown in Figure 5; here we adopted the value at which the function $E_B(k)y(kS)$ drops below 0.1% of its peak value.

The trial function $E_B(k)$ that provides the best fit to the measured $\langle E_{B_{\parallel}} \rangle$ is a slowly decreasing power law described by

$$E_B(k) = C \left(\frac{k}{k_0} \right)^{\alpha}, \quad (15)$$

with $\alpha = -0.37 \pm 0.10$ and $C = (6.8 \pm 0.8) \times 10^{-13} \text{ erg cm}^{-3} \text{ kpc}$. As a reminder, k is the wavenumber defined as $1/\lambda$ and $k_0 = 1 \text{ kpc}^{-1}$. The power-law indices of $\langle E_{B_{\parallel}} \rangle(S)$ (see eq. [5]) and $E_B(k)$ (see eq. [15]) are approximately related through $\beta = 1 + \alpha$. This relation would be exact if the weight function $y(kS)$ were approximated by the step function $u(1 - kS)$, where $u(x)$ is defined such that $u(x) = 0$ for $x < 0$ and $u(x) = 1$ for $x > 0$. Consequently, the uncertainty in α is comparable to the uncertainty in β , i.e., $\simeq 0.10$. Furthermore, since $\langle E_{B_{\parallel}} \rangle(S)$ has been reliably determined over the range $0.5 \text{ kpc} < S < 15 \text{ kpc}$ (see Section 2.1), the validity range of equation (15) is approximately $0.07 \text{ kpc}^{-1} < k < 2 \text{ kpc}^{-1}$.

The rms value of the fluctuating magnetic field with wavenumbers in the above range, obtained by integrating equation (15), is $6.1 \pm 0.5 \mu\text{G}$. We note that this rms field strength is consistent with estimates by previous authors, e.g., via modelling diffuse γ -ray data and synchrotron emission (Strong et al. 2000), via energy equipartition (Berkhuijsen, referenced in Beck et al. 1996), or based on pulsar data and synchrotron data by Heiles (1996). This leads us to believe that equation (1) using pulsar RM and DM data does not significantly underestimate or overestimate the field strength in the ISM, at least on average over a large sample.

3. VALIDITY OF THE UNDERLYING ASSUMPTIONS

We have used the tools of homogeneous and isotropic turbulence theory to derive the spatial power spectrum of magnetic energy in our Galaxy. However, strictly speaking, these are not directly applicable to the problem at hand. Firstly, the spatial variations of the magnetic field at the scales probed here are not all stochastic; some are associated with large-scale coherent features such as supernova remnants or superbubbles and others are associated with the large-scale Galactic spiral structure. In this study, we did not try to distinguish the purely stochastic fluctuations from the coherent variations; all are included in our magnetic energy spectrum. This procedure is justified if the results are taken to represent present-day Galactic averages rather than true statistical averages.

A second, more fundamental, reason is that the magnetic energy distribution is neither homogeneous across the sampled region (it includes spatial variations up to scales approaching the size of the region, which is itself a substantial portion of the Galaxy) nor isotropic (the effects of the disk geometry and the associated vertical stratification are significant at the relevant spatial scales). The most obvious manifestation of the lack of isotropy is the dominant horizontal component of the large-scale magnetic field.

The failure of the assumption of homogeneity is inherent in our scale range. Minter & Spangler (1996) did not encounter the same problem because they studied only small-scale fluctu-

ations, such that they were able to perform statistically meaningful spatial averages over a region which is small enough for turbulence to be assumed homogeneous across it. The downside is that their spectrum applies only to their small region of observations and to small scales. In contrast, our derived spectrum does not constitute a good statistical average. However, since our pulsar pairs are reasonably well distributed throughout the sampled volume, our spectrum may be regarded as a spatial average over the sampled volume – with some bias toward the vicinity of the Sun. Since the sampled volume corresponds roughly to a 120° wedge of the Galactic disk seen from the Galactic center, it is probably representative of the whole disk. In this case, our derived spectrum also provides a good estimate for the Galaxy-wide average spectrum.

The assumption of isotropy is almost unavoidable and routinely made in practice (e.g. Ohno & Shibata 1993; Minter & Spangler 1996), even though it fails both at large scales (for the reason outlined above) and at small scales (due to the presence of the large-scale magnetic field). Here, the use of the isotropy assumption and of the ensuing formulae would be justified if the sky coverage in line-of-sight direction were complete and uniform and if the magnetic spectrum were homogeneous (so as to give all directions the same weight). However, neither condition is fully satisfied. The resulting uncertainty can be estimated once it is realized that the situation we are dealing with is intermediate between 3D isotropic and 2D isotropic (with the magnetic field at all locations and all sightlines being parallel to the Galactic plane). The 2D case can be treated similarly to the 3D case studied in § 2.2 and § 2.3: the expression found for $\langle E_{B_{\parallel}} \rangle(S)$ is identical to equation (13) with the $1/3$ prefactor replaced by $1/2$ and the weight function given by

$$y(kS) \equiv \frac{2}{\pi} \int_0^{\pi kS} \frac{1}{\sqrt{(\pi kS)^2 - x^2}} \left(\frac{\sin x}{x} \right)^2 dx. \quad (16)$$

A numerical fit to Figure 4 then leads to a corresponding equation (15) with $\alpha = -0.39 \pm 0.10$ and $C_{2D} = (8.6 \pm 1.0) \times 10^{-13} \text{ erg cm}^{-3} \text{ kpc}$. This shows that the derived values are not very sensitive to the isotropy assumption. The reason why a similar spectral index is obtained in the 2D and 3D cases is easily understood. In § 2.3, we saw that the spectral index obtained with the step-function approximation to the weight function ($\alpha = \beta - 1 = -0.34$) is close to that obtained with the correct weight function ($\alpha = -0.37$). This indicates that the slope of the energy spectrum depends little on the exact shape of the weight function, but is governed by the relative positions of the cutoff wavenumbers.

Another important assumption implicit in our derivation is the absence of correlation between the fluctuations in electron density and those in magnetic field strength, which allows us to approximate the space-averaged value of B_{\parallel} between two points (eq. [8]) by a density-weighted average (eq. [1] or [2]). This assumption may not be well satisfied in the ISM. Both positive and negative correlations are possible and their net effect is difficult to quantify (Beck et al. 2003). However, as mentioned in § 2.3, our derived rms field strength is consistent with other estimates. In addition, the fluctuation spectral index is affected only if the degree of correlation is scale-dependent.

Finally, individual pulsar distances are uncertain by a large factor, typically $\sim 20\%$, although the overall distance scale is more accurate. The impact on our derived magnetic spectrum is limited by the fact that the values of $\langle E_{B_{\parallel}} \rangle(S)$ were obtained from the average of many measurements of $\overline{B_{\parallel}}^{-2}$.

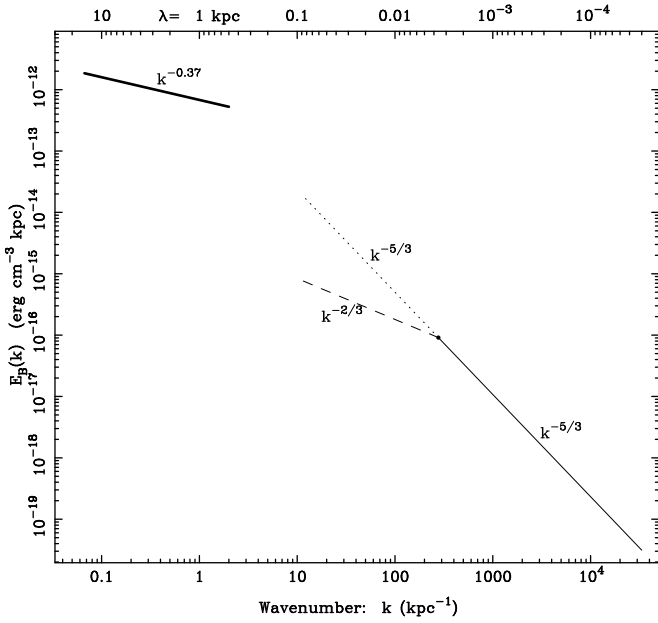


FIG. 6.— Composite magnetic energy spectrum in our Galaxy. The thick solid line is the large-scale spectrum derived in this paper. The thin solid and dashed/dotted lines give the Kolmogorov and 2D-turbulence spectra, respectively, inferred from the Minter & Spangler (1996) study. Their Kolmogorov spectrum, after adjusting to our definition of k , can be written as $E_B(k) = C_K (k/k_0)^{-5/3}$ with $C_K = 9.5 \times 10^{-13} \text{ erg cm}^{-3} \text{ kpc}$ and $k_0 = 1 \text{ kpc}^{-1}$. The 2D-turbulence spectrum is uncertain (see main text); it probably lies between the dashed ($E_B(k) \propto k^{-2/3}$) and dotted ($E_B(k) \propto k^{-5/3}$) lines, which are both scaled to match the Kolmogorov spectrum at $k_{3D} = (4 \text{ pc})^{-1}$.

4. DISCUSSION

We have derived the interstellar magnetic energy spectrum over the scale range $0.5 - 15 \text{ kpc}$, based directly on measurements of pulsar RMs and DMs. The outer scale is a significant fraction of the size of the Galaxy and so contributions from the so-called large-scale (or regular) magnetic field are included. The spectral region covered by our derived spectrum has never been studied observationally before, yet it constitutes a crucial piece of the complete spectrum, whose knowledge is important for our understanding of the behavior and evolution of Galactic magnetic fields.

In Figure 6, we plot our measured spectrum with that inferred from the Minter & Spangler (1996) study at smaller scales. This spectrum has a Kolmogorov slope ($E_B(k) \propto k^{-5/3}$) up to a scale $l_{3D} \sim 4 \text{ pc}$ and an uncertain shape consistent with 2D turbulence between l_{3D} and $l_{2D} \sim 80 \text{ pc}$. If, as suggested by Minter & Spangler (1996), the 2D turbulence is in the form of thin sheets with thickness $\sim l_{3D}$, we could assume that fluctuations with scales larger than l_{3D} persist only if their projected wavelength normal to a sheet, $\lambda \cos \theta$, is less than the sheet's thickness l_{3D} . The fraction of acceptable wave vectors at a given wavenumber k is then $l_{3D}/\lambda = k/k_{3D}$. If the acceptable wave vectors preserve a Kolmogorov spectral energy, the magnetic spectrum in the wavenumber range $k_{2D} - k_{3D}$ is simply the Kolmogorov spectrum multiplied by the above factor, i.e., a $k^{-2/3}$ spectrum. On the other hand, if 2D turbulence means that the spectral energy is simply redistributed without loss into two dimensions, then the Kolmogorov spectrum $\propto k^{-5/3}$ extends out to k_{2D} . The actual situation probably lies between these two extremes.

The two important features emerging from the composite spectrum (Figure 6) are (1) a change in slope from $\alpha = -5/3$ at

the small ($\lesssim 4 \text{ pc}$) scales to $\alpha \simeq -0.37$ at the large ($\gtrsim 0.5 \text{ kpc}$) scales and (2) a possibly significant discontinuity between $\sim 80 \text{ pc}$ and $\sim 0.5 \text{ kpc}$. How do these two features fit with theoretical predictions?

According to our theoretical understanding of the ISM, turbulent energy is injected into the ISM by stellar winds and supernova explosions on scales $\sim 10 - 100 \text{ pc}$. Magnetic energy is then transferred, via a so-called direct cascade, toward smaller and smaller scales. In addition, because interstellar turbulence is helical, there is also an inverse cascade of magnetic helicity toward larger and larger scales, making it possible to amplify or maintain a large-scale magnetic field (Pouquet et al. 1976). Because the quantity that is transferred as a whole in the domain of the inverse cascade is magnetic helicity ($H_B(k) \propto E_B(k)/k$) rather than magnetic energy, the corresponding spectrum is flatter than in the domain of the direct cascade. Therefore, our finding a flatter spectrum at the larger scales is consistent with the inverse cascade theory.

However, the value obtained for the spectral index ($\alpha \simeq -0.37$) differs from current theoretical estimates. In the theory of 3D MHD helical turbulence developed by Pouquet et al. (1976), a numerical solution of the evolution equation for the magnetic energy spectrum yields $E_B(k) \propto k^{-1}$ at scales larger than the injection scale. As shown by these authors, the same spectral slope is obtained by applying a dimensional Kolmogorov-type argument to the inverse cascade of magnetic helicity. Direct numerical simulations do not yet convey an unambiguous or consistent picture. Balsara & Pouquet (1999) obtained numerical spectra consistent with the k^{-1} theoretical prediction. In contrast, in the simulations of Brandenburg (2001), a wave of spectral magnetic energy propagates toward smaller k under a k^{-1} envelope, but no k^{-1} spectrum actually develops. Instead, magnetic energy builds up at the largest scales and a secondary peak appears at the injection scale. Maron & Blackman (2002) showed that the actual shape of the magnetic energy spectrum depends in fact quite sensitively on the level of fractional kinetic helicity with which the turbulence is forced. According to their simulations, high levels of kinetic helicity lead to double-peaked spectra similar to that obtained by Brandenburg (2001), whereas low levels of kinetic helicity give rise to a single peak at the small resistive scale. It is clear that one has to be extremely cautious when trying to apply numerical spectra to the real Galactic magnetic field. Current simulations are still highly idealized (e.g., uniform background medium, incompressible or isothermal gas, periodic boundary conditions), and they neglect potentially important factors such as the true nature of turbulent forcing, the presence of large-scale shear, and the actual boundaries of the Galactic disk. Another difficulty is that the saturated spectra obtained numerically emerge after resistivity comes into play, whereas the Galaxy is probably not yet in the resistive regime (Blackman, private communication).

The discontinuity appearing between the $<100 \text{ pc}$ and $>0.5 \text{ kpc}$ scales in the composite spectrum of Figure 6 can be partly explained by the fact that the different parts of the spectrum apply to different Galactic regions. As discussed in § 3, our portion of the spectrum was obtained from a magnetic energy average over about one third of the inner Galactic disk, while that of Minter & Spangler (1996) was obtained from a small high-latitude region in the outer Galaxy, where the fields are presumably much weaker than in the inner disk. However, if the 2D-turbulence portion of the spectrum is as flat as $k^{-2/3}$, the observed discontinuity is so severe that it suggests a genuine excess in the Galac-

tic magnetic energy spectrum at large scales. This excess compared to the amount expected from the inverse cascade alone could indicate that most of the energy input to the large-scale magnetic field occurs directly at large scales. This interpretation would be consistent with the standard Galactic dynamo theory, in which the large-scale magnetic field is amplified or maintained through the combined action of small-scale helical turbulence, presumably via the inverse cascade leading to the so-called α -effect, and large-scale shear, typically associated with the Galactic differential rotation (e.g., Parker 1971; Vainshtein & Ruzmaikin 1971). It is widely believed that the large-scale shear acts much more efficiently than the helical turbulence (e.g., Parker 1971; Ruzmaikin et al. 1988; Brandenburg et al. 1992; Ferrière & Schmitt 2000; Blackman 2000), especially when the spiral structure of the Galaxy and the streaming motions along spiral arms are taken into account (e.g., Rohde et al. 1999; Elstner et al. 2000). A more extreme point of view would be to consider that the large-scale magnetic field is not affected at all by the small-scale turbulent field and that all the energy contained in the large-scale field is directly injected at large scales. Various scenarios have been proposed in this spirit, such as protogalactic collapse and subsequent shearing by the Galactic differential rotation with rapid ambipolar diffusion (Kulsrud 1986) or protogalactic collapse and subsequent excitation of spiral arms and bars resulting in nonaxisymmetric, not-perfectly-azimuthal motions (Lesch & Chiba 1997).

ACKNOWLEDGMENTS

We thank an anonymous referee for an extensive report which helped us improve the clarity of the paper. We also thank Sun Xiaohui, You Xiaopeng and Xu Jianwen for helpful discussions. JLH is supported by the National Natural Science Foundation (NNSF) of China (10025313) and the National Key Basic Research Science Foundation of China (G19990754) as well as the partner group of MPIfR at NAOC. The Parkes radio telescope is part of the Australia Telescope which is funded by the Commonwealth Government for operation as a National Facility managed by CSIRO.

REFERENCES

- Armstrong, J. W., Rickett, B. J., & Spangler, S. R. 1995, *ApJ*, 443, 209
 Balsara, D. & Pouquet, A. 1999, *Physics of Plasmas*, 6, 89
 Beck, R., Brandenburg, A., Moss, D., Shukurov, A., & Sokoloff, D. 1996, *ARA&A*, 34, 155
 Beck, R., Shukurov, A., Sokoloff, D., & Wielebinski, R. 2003, *A&A*, in press.
 Blackman, E. G. 2000, *ApJ*, 529, 138
 Brandenburg, A. 2001, *ApJ*, 550, 824
 Brandenburg, A., Donner, K. J., Moss, D., Shukurov, A., Sokoloff, D. D., & Tuominen, I. 1992, *A&A*, 259, 453
 Cordes, J. M. & Lazio, T. J. W. 2003, *ApJ*, submitted
 Crovisier, J. & Dickey, J. M. 1983, *A&A*, 122, 282
 Deshpande, A. A., Dwarakanath, K. S., & Goss, W. M. 2000, *ApJ*, 543, 227
 Dickey, J. M., McClure-Griffiths, N. M., Stanimirović, S., Gaensler, B. M., & Green, A. J. 2001, *ApJ*, 561, 264
 Elstner, D., Otmianowska-Mazur, K., von Linden, S., & Urbanik, M. 2000, *A&A*, 357, 129
 Ferrière, K. & Schmitt, D. 2000, *A&A*, 358, 125
 Green, D. A. 1993, *MNRAS*, 262, 327
 Hamilton, P. A. & Lyne, A. G. 1987, *MNRAS*, 224, 1073
 Han, J. L., Manchester, R. N., Lyne, A. G., & Qiao, G. J. 2002, *ApJ*, 570, L17
 Han, J. L., Manchester, R. N., & Qiao, G. J. 1999, *MNRAS*, 306, 371
 Han, J. L. & Qiao, G. J. 1994, *A&A*, 288, 759
 Heiles, C. 1996, in *ASP Conf. Ser. 97: Polarimetry of the Interstellar Medium*, 457
 Indrani, C. & Deshpande, A. A. 1998, *New Astronomy*, 4, 33
 Kulsrud, R. 1986, in *Plasma Astrophysics*, ed. T. Guyenne & L. Zeleny (ESA Publ. SP-251, Paris), 531–537
 Lesch, H. & Chiba, M. 1997, *Fundamentals of Cosmic Physics*, 18, 273
 Maron, J. & Blackman, E. G. 2002, *ApJ*, 566, L41
 Minter, A. H. & Spangler, S. R. 1996, *ApJ*, 458, 194
 Ohno, H. & Shibata, S. 1993, *MNRAS*, 262, 953
 Parker, E. N. 1971, *ApJ*, 163, 255
 Pouquet, A., Frisch, U., & Leorat, J. 1976, *Journal of Fluid Mechanics*, 77, 321
 Qiao, G. J., Manchester, R. N., Lyne, A. G., & Gould, D. M. 1995, *MNRAS*, 274, 572
 Rand, R. J. & Kulkarni, S. R. 1989, *ApJ*, 343, 760
 Rand, R. J. & Lyne, A. G. 1994, *MNRAS*, 268, 497
 Rohde, R., Rüdiger, G., & Elstner, D. 1999, *A&A*, 347, 860
 Ruzmaikin, A. A., Sokolov, D. D., & Shukurov, A. M. 1988, *Magnetic fields of galaxies* (Kluwer Academic)
 Simard-Normandin, M. & Kronberg, P. P. 1980, *ApJ*, 242, 74
 Simonetti, J. H. & Cordes, J. M. 1986, *ApJ*, 310, 160
 Simonetti, J. H., Cordes, J. M., & Spangler, S. R. 1984, *ApJ*, 284, 126
 Strong, A. W., Moskalenko, I. V., & Reimer, O. 2000, *ApJ*, 537, 763
 Vainshtein, S. I. & Ruzmaikin, A. A. 1971, *Astron. Zh.*, 48, 902, [*Sov. Astron.*, 15, 714 (1972)]